JAAS

ROYAL SOCIETY OF CHEMISTRY

PAPER

View Article Online
View Journal | View Issue

Cite this: *J. Anal. At. Spectrom.*, 2026, **41**, 2060

Development of a plasma injection probe for deep tissue drug analysis

Yuya Shimizu,[a] Masaya Tahara,[a] Akane Yaida,[a] Yukiko Moriiwa,[b] Toshihiro Takamatsu,*[c] Atsushi Shoji[b] and Akitoshi Okino[a]

Anticancer drugs and other pharmaceuticals achieve maximal therapeutic efficacy with minimal side effects when delivered to the target site at an appropriate concentration. Accordingly, quantifying the amount of drug reaching the target tissue is essential for evaluating pharmacological effectiveness. However, direct measurement of a drug concentration within specific tissues *in vivo* remains technically challenging. In this study, a plasma injection probe incorporating an ultra-small plasma source inside a syringe needle was developed, and its fundamental performance was evaluated using 4-isopropylantipyrine as a model analyte. First, an ultra-small plasma source with an outer diameter of approximately 700 μm, suitable for integration into an injection needle, was fabricated. Plasma irradiation of a biological tissue-mimicking sample surface demonstrated that helium yielded the highest signal intensity among the tested plasma generation gases. In addition, the introduction of 2% hydrogen further enhanced analytical sensitivity. The measured gas temperature was approximately 22–23 °C, indicating suitability for potential *in vivo* application. Subsequently, the plasma injection probe was inserted into a biological tissue-mimicking sample to evaluate its capability to detect drugs within the sample interior. When the plasma gas flow rate was varied, the signal intensity reached a maximum at 100 mL min^{-1}, and the limit of detection was approximately 10 ppm. Furthermore, the depth resolution of the plasma injection probe was determined to be 0.4 mm.

Received 12th December 2025
Accepted 9th April 2026

DOI: 10.1039/d5ja00495k

rsc.li/jaas

1 Introduction

In recent years, advances in understanding disease mechanisms have increased the need for molecularly targeted therapies that selectively act on tissues involved in disease onset and progression, thereby reducing patient burden.[1–4] In particular, anticancer drugs eliminate cancer cells by inhibiting cell division or inducing DNA damage. However, systemic administration exposes normal cells to the drug, resulting in adverse effects. Minimizing systemic exposure is therefore essential.[5–7] Consequently, molecularly targeted drugs[8,9] that selectively act on specific disease-causing molecules within the body, and drug delivery systems (DDS) that enhance drug efficacy and suppress side effects by efficiently delivering drugs to target sites, are attracting significant attention.[10–13] The development of such therapeutics requires characterization of their pharmacokinetics, including their localization within lesions and their ability to penetrate deep tissues. Accordingly, numerous studies have investigated the *in vivo* distribution of these drugs.[14–16]

Current methods for evaluating drug concentrations at defined sites in the body include tissue sampling through biopsy,[17–19] microdialysis using thin probes inserted into tissue to collect drugs from interstitial fluid,[20–22] and imaging techniques that track radiolabeled or fluorescently labeled drugs to determine their distribution and concentration over time after administration.[23–25] In biopsy-based analysis, various analytical techniques, including immunostaining and mass spectrometry, can be applied. However, the invasiveness of biopsy limits the amount of tissue that can be clinically collected, making it difficult to obtain a comprehensive understanding of drug distribution within the entire lesion. Microdialysis enables drug analysis at specific locations *in vivo* by inserting a probe and collecting interstitial fluid through the dialysis membrane. Nevertheless, the collected drug concentration is lower than the true extracellular concentration, which complicates highly sensitive quantification. In addition, the probes are thin and may fracture when inserted into rigid tissues such as tumors or muscles. Imaging-based approaches using labeled drugs allow assessment of drug distribution within the body, yet the range of analysable drugs is restricted, and the labeled compounds themselves may pose safety concerns.

Therefore, our group focused on the Atmospheric Plasma Soft Ablation (APSA) method,[26–30] which our laboratory previously developed for the non-destructive desorption and analysis

[a]*Laboratory for Future Interdisciplinary Research of Science and Technology (FIRST), Institute of Sciences Tokyo, 4259-J2-32 Nagatsuta, Midori-ku, Yokohama, Kanagawa, 226-8502, Japan*

[b]*Tokyo University of Pharmacy and Life Sciences, 1432-1 Horinouch, Hachioji-shi, Tokyo, 192-0392, Japan*

[c]*Health and Medical Research Institute, National Institute of Advanced Industrial Science and Technology, Tsukuba, Ibaraki, Japan. E-mail: takamatsu@rs.tus.ac.jp*

of substances adhering to material surfaces. This technique uses a plasma source capable of generating low temperature plasma at atmospheric pressure and about room temperature. Plasma irradiation onto the material surface causes adhered drug molecules to desorb, after which the desorbed molecules are ionized by protons originating from ambient water vapor and introduced into a mass spectrometer for analysis. By varying the irradiation position, this method enables wide area mapping analysis. It also allows on-site quantification of drug concentrations in diseased tissue without the need for complex sample pretreatment. Therefore, we propose a plasma injection probe that incorporates a plasma source capable of generating atmospheric-pressure low-temperature plasma within an injection needle. This plasma can be irradiated directly into the body, enabling desorption and ionization of drugs and thus allowing real-time *in vivo* drug analysis based on the APSA method. With this device, inserting the injection needle into a target lesion and irradiating the site with plasma would desorb and ionize drug molecules at the needle tip. The gas carrying these desorbed molecules can then be extracted through the internal gap of the injection needle and transported outside the probe for introduction into a mass spectrometer.

In this study, we developed an ultra-small plasma source suitable for integration into an injection needle. We optimized analytical conditions by measuring drug containing surfaces while varying the gas type and other parameters. Furthermore, we constructed the plasma injection probe by incorporating this ultra-small plasma source into the injection needle. To assess its fundamental performance, we analysed drugs within a biological tissue-mimicking sample prepared by dispersing drug compounds in agar.

2 Experimental

2.1 Development of the plasma injection probe

Fig. 1 shows a conceptual diagram of the plasma injection probe developed for real-time analysis of drug concentrations at specific locations within biological tissue. The device incorporates a plasma source capable of generating atmospheric-pressure low-temperature plasma inside a 16 G needle (inner diameter: 1.25 mm; outer diameter: 1.61 mm), enabling the desorption and ionization of drug molecules. To develop this device, an ultra-small plasma source with an outer diameter of approximately 700 μm, suitable for integration into the injection needle, was fabricated. A schematic of the ultra-small plasma source is shown in Fig. 2.

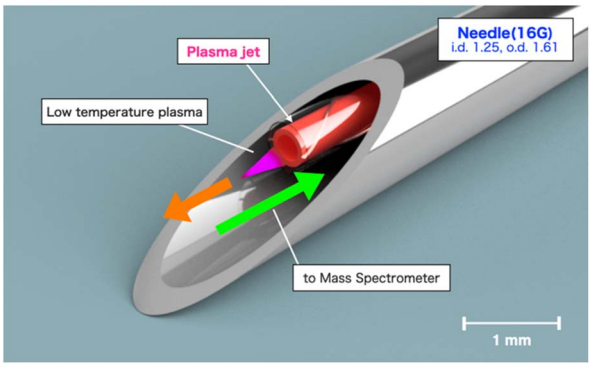

Fig. 1 Schematic diagram of the plasma injection probe.

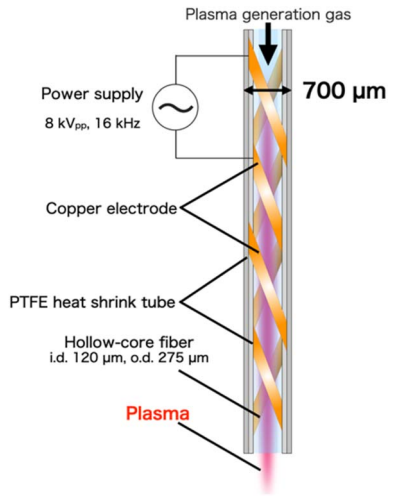

Fig. 2 Schematic diagram of the ultra-small plasma source.

The plasma source was constructed by insulating a hollow optical fiber (inner diameter: 120 μm; outer diameter: 275 μm; HC-1550, Thorlabs Inc.) with a PTFE heat-shrink tubing (SLW-AWG-33HS, HAGITECH LTD). A 50-μm-thick copper wire was then wound spirally around the outer surface of the fiber as an electrode, followed by re-insulation using a PTFE heat-shrink tubing (SLW-SWG-32HS, HAGITECH LTD) arranged in a helical configuration over the electrode. All materials used in this device are expected to be compatible with sterilization methods similar to those applied to general medical devices. In particular, even when high-pressure steam sterilization (autoclaving) is used, the operating temperature is lower than the shrink temperature of the heat-shrink tubing. Therefore, the fabricated ultra-small plasma source is expected to be sterilized without affecting its structure or performance.

To generate plasma, a plasma-generation gas was introduced through the ultra-small plasma source, and an alternating voltage of 8 kV at 16 kHz, monitored using an oscilloscope (TBS 2000B Series, Tektronix) and a high-voltage probe (HVP-30Pro, PINTEX), was applied to the copper electrode. The completed ultra-compact plasma jet was then integrated into a 16 G injection needle to verify the feasibility of plasma generation within the needle.

2.2 Optimization of plasma irradiation

To evaluate the applicability of the APSA method using plasma generated by the fabricated ultra-small plasma source, a biological tissue-mimicking sample was prepared and analysed for drug molecules on its surface. The experimental setup is shown in Fig. 3.

The biological tissue-mimicking sample was prepared using agar. Agar powder was dissolved in purified water at

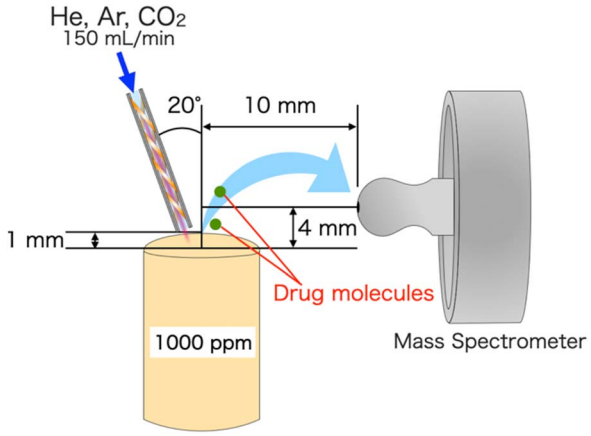

Fig. 3 Experimental setup for evaluating plasma irradiation conditions.

a concentration of 1.5 g per 100 mL, and 4-isopropylantipyrine (Tokyo Chemical Industry Co., Ltd) was added as the target analyte at a concentration of 1000 ppm. The mixture was autoclaved at 121 °C for 15 min and then allowed to solidify at 20 °C for 24 h to obtain the biological tissue-mimicking sample. 4-Isopropylantipyrine was selected as the model analyte because it has been reported to exhibit high analytical sensitivity and stable signal responses in the previously reported APSA method. For surface analysis, plasma was generated using argon, carbon dioxide, or helium at a flow rate of 150 mL min^{-1} and a discharge voltage of 6 kVpp at 16 kHz. The biological tissue-mimicking sample was positioned in front of the ion inlet of the mass spectrometer (amaZon SL-AI, Bruker), with its surface located 4 mm below the inlet. The ultra-small plasma source was placed 1 mm above the sample surface, oriented at a 20° angle, and positioned 10 mm from the ion inlet. Plasma irradiation desorbed and ionized drug molecules, which were subsequently introduced into the mass spectrometer. Because the APSA method relies on protonation by protons originating from water vapor in the air, hydrogen addition was expected to enhance ionization efficiency. To examine this effect, plasma was generated using helium containing 0–5% hydrogen at a total flow rate of 150 mL min^{-1}, and the resulting signal intensity was evaluated.

The gas temperature of the plasma was also measured to determine whether the plasma source could be safely applied to the human body. Plasma generation conditions were identical to those used for the hydrogen-addition experiments. As shown in Fig. 4, plasma temperature was measured for 90 s after ignition using a fiber optic temperature sensor (PRB-G40-02M-ST-C, Osensa Innovations) connected to a fiber-optic transmitter (FTX-200-LUX+, Osensa Innovations). The sensor tip was positioned 0.5 mm from the outlet of the ultra-small plasma source.

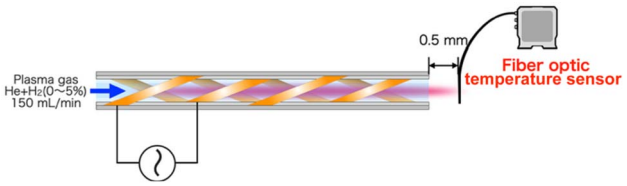

Fig. 4 Experimental setup for measuring plasma gas temperature.

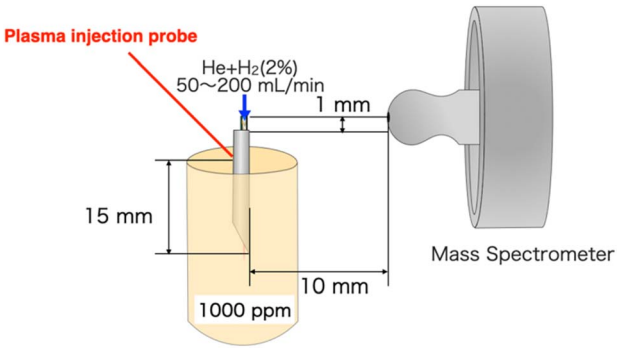

Fig. 5 Experimental setup for plasma-generation gas flow rate.

2.3 Analysis of biological tissue-mimicking samples

To evaluate the capability of the developed plasma injection probe for *in vivo* analysis, the probe was inserted into a biological tissue simulant and subjected to analytical testing. The biological tissue simulant was prepared following the same procedure described in the previous section. The experimental setup for the analysis using the plasma injection probe is shown in Fig. 5. As illustrated in Fig. 5, the biological tissue-mimicking sample was positioned upstream of the mass spectrometer, and the plasma injection probe was inserted 15 mm into the sample at a location 10 mm from the ion inlet. Plasma irradiation was applied to desorb and ionize drug molecules within the biomimetic matrix. To examine the relationship between the plasma-generating gas flow rate and analytical sensitivity, helium containing 2% hydrogen was introduced at flow rates ranging from 50 to 200 mL min^{-1} to generate the plasma.

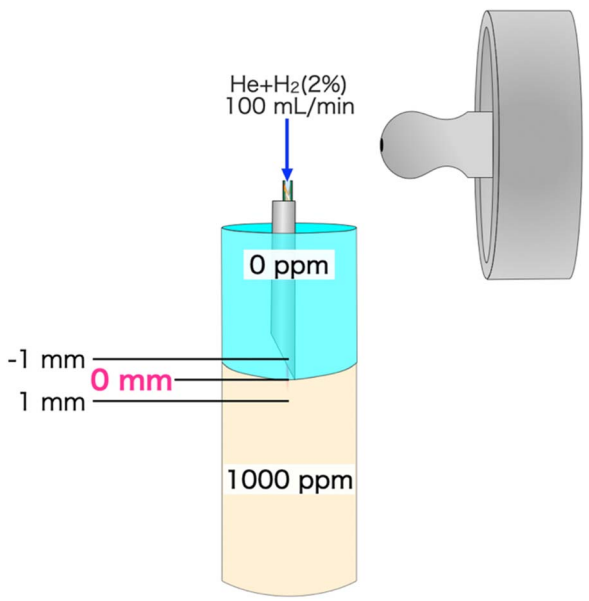

Fig. 6 Experimental setup for depth resolution.

Subsequently, to assess the depth resolution of the plasma injection probe, a biological tissue-mimicking sample with a spatially varied drug concentration was prepared and analysed. The experimental setup is shown in Fig. 6. In this experiment, drug-free agar was layered atop a 1000 ppm biological tissue-mimicking sample. The plasma injection probe was fixed in place, and analyses were conducted at positions 1 mm above and below the interface between the two layers, with the boundary defined as 0 mm.

3 Results and discussion

3.1 Plasma generation using the plasma injection probe

Fig. 7(a) shows the plasma generated using the developed ultra-small plasma source, and Fig. 7(b) presents plasma generation inside a biological tissue-mimicking sample using the plasma injection probe, in which the ultra-small plasma source is integrated into a syringe needle. As shown in Fig. 7, the plasma injection probe successfully generated plasma inside the biological tissue-mimicking sample. In addition, no electrical discharge was observed between the ultra-small plasma source incorporated in the syringe needle and the inner wall of the needle. These results indicate that the plasma injection probe does not pose a risk of electric shock from the needle when inserted into the human body for analytical purposes.

The needle employed in the plasma injection probe developed in this study was 16 G. In core needle biopsy, sampling with a 14 G needle (inner diameter: 1.69 mm; outer diameter: 2.11 mm) has been reported for soft tissue sarcomas[31] and neuroblastomas,[32] suggesting that the plasma injection probe is suitable for drug analysis in such deep-seated tissues. In contrast, in the thyroid, finer needles of 18 G (inner diameter: 0.90 mm; outer diameter: 1.26 mm) or smaller are commonly used.[33,34] Considering that the diameter of the ultra-small plasma source is approximately 700 μm, the probe can be directly applied to an 18 G needle. However, the gap between the plasma source and the inner wall of the needle becomes smaller, which may affect the transport efficiency and the amount of gas containing the drug introduced into the mass spectrometer. Therefore, it is necessary to adjust both the flow rate of the plasma-generation gas and the suction flow rate of the drug-containing gas. For application to needles thinner than 18 G, further miniaturization of the plasma source would be required. In this case, since the plasma generation mechanism remains the same, the stability and temperature of the plasma are not expected to change significantly. However, higher fabrication precision would be required due to the miniaturization of the electrode structure, and therefore optimization of the development process would be necessary.

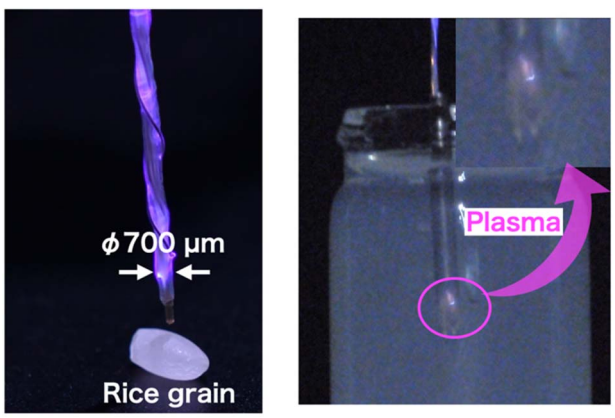

Fig. 7 Photograph of plasma generation.

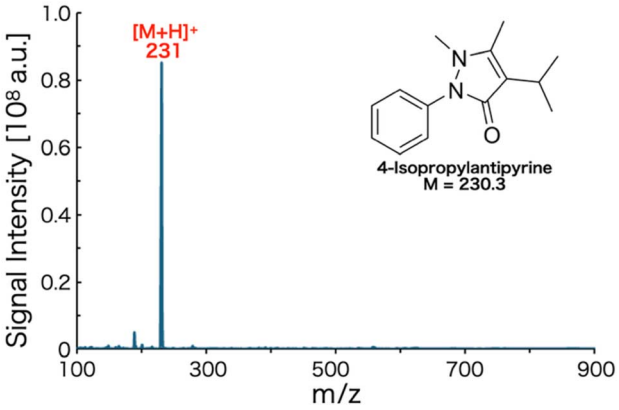

Fig. 8 Analysis result of the sample surface.

3.2 Optimization of plasma conditions

The result of the surface analysis of the biological tissue-mimicking sample using helium plasma generated by the ultra-small plasma source is shown in Fig. 8. As shown in Fig. 8, the developed ultra-small plasma source successfully enabled the surface analysis of the biomimetic sample. A signal peak was observed at $m/z = 231$ rather than at the nominal mass of 4-isopropylantipyrine ($m/z = 230$). This shift is attributed to protonated molecular ions formed through the attachment of protons derived from airborne water vapor within the mass spectrometer.

Fig. 9 compares the analytical results obtained using plasma generated from different discharge gases. The error bars

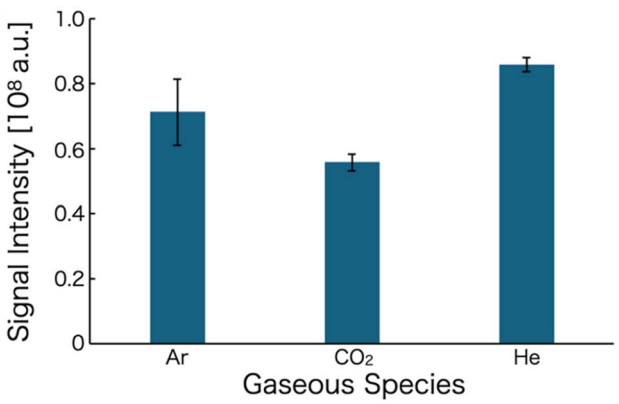

Fig. 9 Signal intensity for each gas type.

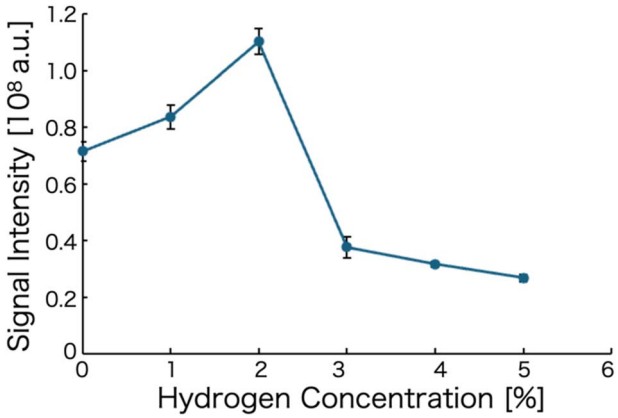

Fig. 10 Signal intensity at each hydrogen concentration.

represent the standard deviation. Among the argon, carbon dioxide, and helium plasmas, helium produced the highest signal intensity. This is likely because, for molecular gases such as carbon dioxide, part of the supplied energy is consumed in molecular dissociation,[35] resulting in fewer energetic ions capable of inducing desorption and ionization of the drug molecules. Furthermore, the higher ionization energy of helium relative to argon[36] is presumed to yield a greater population of ions with sufficient energy for analyte desorption and ionization, thereby producing stronger signals.

Helium is an inert gas with low chemical reactivity and is therefore considered to have minimal biological impact. Moreover, previous studies have reported the irradiation of biological tissues using helium-based low-temperature plasma, with no significant adverse effects observed.[37–39] However, when plasma is irradiated inside biological tissues, as proposed in this study, additional verification of safety and operating conditions will be necessary.

The analytical results obtained while varying the hydrogen concentration in the plasma generation gas are presented in Fig. 10. The error bars represent the standard deviation. The signal intensity increased progressively as the hydrogen concentration was raised from 0% to 2% but further increases to 3–5% resulted in a marked decrease in signal intensity. These results indicate that the optimal hydrogen concentration for drug analysis using the ultra-small plasma source is approximately 2%. The enhancement observed up to 2% is attributed to the additional supply of protons from hydrogen, which supplements the proton contribution from atmospheric water vapor and thereby increases the number of ionized drug molecules. In contrast, the decline in signal intensity at hydrogen concentrations of 3–5% is likely due to a reduction in helium plasma density and the energy consumption associated with hydrogen atom ionization, ultimately decreasing the efficiency of analyte desorption and ionization.

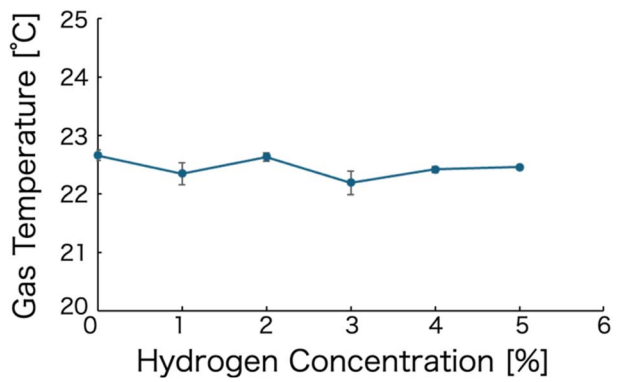

Fig. 11 Gas temperature at each hydrogen concentration.

The average gas temperatures of plasma generated with 0–5% hydrogen admixture, measured 60–90 s after ignition, are presented in Fig. 11. The error bars represent the standard deviation. Under all conditions, the gas temperature remained nearly constant at approximately 22–23 °C. This stability is attributed to the dielectric barrier discharge (DBD) mechanism utilized in the ultra-small plasma source, in which intermittent discharges occur because the applied AC voltage periodically interrupts the discharge. Such intermittent behavior reduces the frequency of particle collisions within the plasma and thereby suppresses gas heating.[40] Based on these results, the plasma generated by the ultra-small plasma source developed in this study is considered to be at a temperature suitable for irradiation of living tissue. Plasma is known to generate reactive oxygen and nitrogen species (ROS/RNS), which may cause damage to surrounding tissues. In the analytical configuration using the plasma injection probe developed in this study, however, the probe is inserted directly into the biological tissue, which is expected to minimize the generation of ROS/RNS originating from ambient air. In addition, since helium and hydrogen are used as the plasma generation gases, the formation of oxygen- and nitrogen-derived reactive species from the plasma gas itself is expected to be limited. Nevertheless, ROS/RNS could potentially be generated through interactions with surrounding biological substances, such as blood. Therefore, further investigation of these effects will be necessary in future studies.

3.3 Analysis of drugs inside a biological tissue-mimicking sample using the plasma injection probe

The plasma injection probe was fabricated using the developed ultra-small plasma source. Fig. 12 shows the results of drug analysis inside a biological tissue-mimicking sample while varying the plasma-generating gas flow rate from 50 to 200 mL min^{-1}. The error bars represent the standard deviation. This study demonstrates, for the first time, that the injection-type mechanism enables the analysis of drugs within biological tissue-mimicking samples using atmospheric-pressure low-temperature plasma. This finding highlights the potential application of this approach for drug analysis in biological tissues and represents a significant advancement. Moreover, unlike conventional tissue biopsy, this method does not require sample extraction, suggesting the feasibility of analysing larger tissue regions. Furthermore, unlike microdialysis, this technology is expected to enable analysis of hard tissues because the probe is rigid. However, to minimize invasiveness, further miniaturization is required.

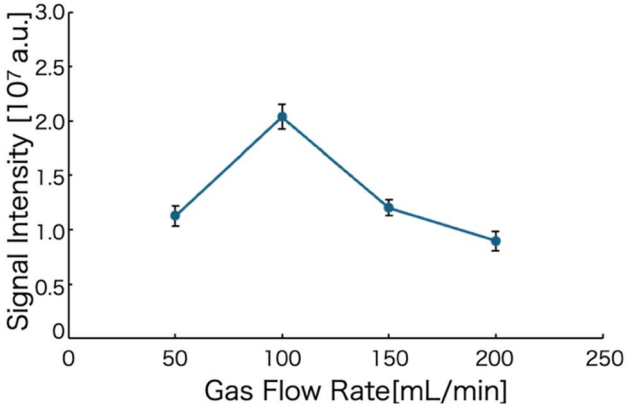

Fig. 12 Signal intensity at each gas flow rate.

When the flow rate was between 50 and 100 mL min^{-1}, the signal intensity increased with increasing flow rate. In contrast, further increases in flow rate from 100 to 200 mL min^{-1} resulted in a decrease in signal intensity. Consequently, the maximum signal intensity was obtained at a flow rate of 100 mL min^{-1}. The enhancement in signal intensity at lower flow rates is attributed to an increase in the density of helium atoms, which in turn increases the number of active species in the plasma and promotes the desorption and ionization of drug molecules from the biological tissue-mimicking sample. The decrease in signal intensity at higher flow rates is likely due to an increase in gas velocity, which shortens the residence time in the plasma-generation region and limits the energy imparted to the gas, thereby reducing the number of active species produced. In addition, the limit of detection (LOD), estimated using a signal-to-noise ratio of 3 based on the noise level around m/z 237–238, was approximately 10 ppm at a flow rate of 100 mL min^{-1}.

Fig. 13 shows the depth-resolved measurements obtained by varying the insertion depth of the plasma injection probe into the biological tissue-mimicking sample. The error bars represent the standard deviation. No signal was observed at an insertion depth of 0 mm, whereas a detectable signal first appeared at 0.2 mm. A signal intensity proportional to the drug concentration was obtained at 0.4 mm. These results indicate that the plasma injection probe provides a depth resolution of approximately 0.4 mm. This resolution is considered adequate for assessing the localized distribution of drugs in soft tissues, such as subcutaneous tissue and tumors, as well as in parenchymal organs including the liver and kidneys. Notably, drug concentrations in biological tissues are known to exhibit heterogeneous distributions on the scale of several hundred micrometers.[41,42] The resolution of the present probe is therefore suitable for localized evaluation of concentration gradients and drug penetration depths within such micro-regions. Nevertheless, analyzing concentration distributions in tissues exhibiting even finer-scale heterogeneity, such as the brain,[43] or in structures with extremely thin layers, such as blood vessel walls, remains challenging.

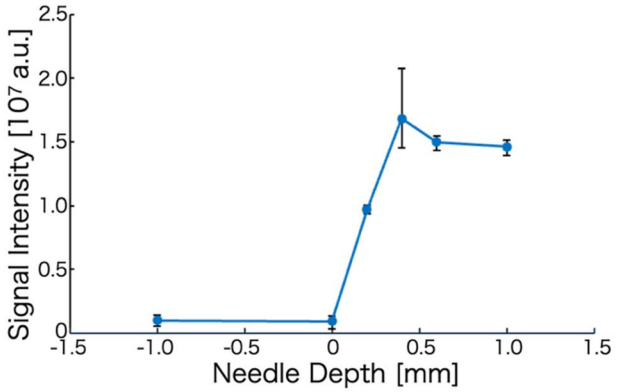

Fig. 13 Signal intensity at each depth.

4 Conclusions

In this study, we developed a plasma injection probe for on-site analysis of drug concentrations in deep tissues. First, an ultra-small plasma source with an outer diameter of approximately 700 μm was fabricated so that it could be integrated into a 16 G injection needle. Plasma generation conditions were then optimized for high-sensitivity drug analysis, and helium containing 2% hydrogen produced the highest signal intensity. The plasma temperature was approximately 22–23 °C, indicating that the plasma can be safely applied to biological tissues.

Furthermore, we examined how variations in the gas flow rate of the plasma injection probe affected analytical performance within a biological tissue-mimicking sample.

This study demonstrated that the plasma injection probe enables high-sensitivity, on-site mapping analysis over a defined area by adjusting the plasma irradiation position, thereby indicating its potential applicability to the analysis of specific tissues within the human body. However, in this study, an agar-based tissue-mimicking sample was used as the analytical target. Therefore, components present in real biological tissues, such as proteins and lipids, were not included in the sample. These components may affect analytical performance through interactions with drug molecules and matrix effects during the ionization process, potentially leading to reduced analytical sensitivity. However, these effects may be partially mitigated by optimizing measurement parameters such as the gas flow rate and suction conditions. In future work, evaluations using real biological tissues will be conducted to further verify the applicability of the proposed method to biological samples.

In the present work, a biological tissue-mimicking sample placed 10 mm from the mass spectrometer ion inlet was analysed. For practical applications, however, analysis at greater distances will be required. To address this need, we are currently developing a method for transporting drug molecules desorbed by the plasma injection probe to the mass spectrometer over longer distances.

The plasma injection probe developed in this study is intended for the analysis of molecular-targeted drugs, such as anticancer agents, at diseased sites within biological tissues. However, in the present work, only 4-isopropylantipyrine was analysed as a model compound. Therefore, it will be necessary

to evaluate analytical characteristics, including the limit of detection and signal stability, for clinically used anticancer drugs with different molecular weights and structures, such as imatinib and 5-fluorouracil.

While this study focused on bioanalytical applications, the plasma injection probe may also be applicable to depth-resolved concentration analysis, such as investigating pollutants penetrating geological formations or the distribution of additives within food products during molecular analysis.

Conflicts of interest

There are no conflicts to declare.

Data availability

Data for this article are available at Figshare repository at DOI: https://doi.org/10.6084/m9.figshare.30862121.

Acknowledgements

This work was supported by JSPS KAKENHI Grant Number 22K19044 and the Nakatani Foundation for Advancement of Measuring Technologies in Biomedical Engineering under the Research Grant Program for Young Scientists (Grant Number 2023S250).

Notes and references

1 X. Ke and L. Shen, *Front. Lab. Med.*, 2017, **1**, 69–75.
2 L. Zhong, Y. Li, L. Xiong, W. Wang, M. Wu, T. Yuan, W. Yang, C. Tian, Z. Miao, T. Wang and S. Yang, *Signal Transduct. Targeted Ther.*, 2021, **6**, 1–48.
3 H.-Y. Min and H.-Y. Lee, *Exp. Mol. Med.*, 2022, **54**, 1670–1694.
4 T. C. Ezike, U. S. Okpala, U. L. Onoja, C. P. Nwike, E. C. Ezeako, O. J. Okpara, C. C. Okoroafor, S. C. Eze, O. L. Kalu, E. C. Odoh, U. G. Nwadike, J. O. Ogbodo, B. U. Umeh, E. C. Ossai and B. C. Nwanguma, *Heliyon*, 2023, **9**, 6.
5 B. A. Chabner and T. G. Roberts, *Nat. Rev. Cancer*, 2005, **5**, 65–72.
6 D. Peer, J. M. Karp, S. Hong, O. C. Farokhzad, R. Margalit and R. Langer, *Nat. Nanotechnol.*, 2007, **2**, 751–760.
7 D. Hanahan and R. A. Weinberg, *Cell*, 2011, **144**, 646–674.
8 D. Aggarwal, J. Yang, M. A. Salam, S. Sengupta, M. Y. Al-Amin, S. Mustafa, M. A. Khan, X. Huang and J. S. Pawar, *Front. Immunol.*, 2023, **14**, 123073.
9 R. Wang, B. Hu, Z. Pan, C. Mo, X. Zhao, G. Liu, P. Hou, Q. Cui, Z. Xu, W. Wang, Z. Yu, L. Zhao, M. He, Y. Wang, C. Fu, M. Wei and L. Yu, *J. Hematol. Oncol.*, 2025, **18**, 51.
10 K. Ulbrich, K. i. Holá, V. Šubr, A. Bakandritsos, J. í. Tuček and R. Zbořil, *Chem. Rev.*, 2016, **116**, 5338–5431.
11 T. Iwamoto, *Biol. Pharm. Bull.*, 2013, **36**, 715–718.
12 G. Tiwari, R. Tiwari, B. Sriwastawa, L. Bhati, S. Pandey, P. Pandey and S. K. Bannerjee, *Int. J. Pharm. Investig.*, 2012, **2**, 2–11.
13 W. B. Liechty, D. R. Kryscio, B. V. Slaughter and N. A. Peppas, *Annu. Rev. Chem. Biomol. Eng.*, 2010, **1**, 149–173.
14 S. Senekowitsch, P. Schick, B. Abrahamsson, P. Augustijns, T. Gießmann, H. Lennernäs, C. Matthys, L. Marciani, X. Pepin, A. Perkins, M. Feldmüller, S. Sulaiman, W. Weitschies, C. G. Wilson, M. Corsetti and M. Koziolek, *Pharmaceutics*, 2022, **14**, 801.
15 P. M. Glasman and V. R. Musykantov, *J. Pharmacol. Exp. Ther.*, 2019, **370**, 570–580.
16 X. Meng, J. Yao and J. Gu, *J. Pharm. Anal.*, 2025, **15**, 101070.
17 A. Nilsson, R. J. A. Goodwin, M. Shariatogorji, T. Vallianatou, P. J. H. Webborn and P. E. Andrén, *Anal. Chem.*, 2015, **87**, 1437–1455.
18 A. Römpp, S. Guenther, Z. Takats and B. Spengler, *Anal. Bioanal. Chem.*, 2011, **401**, 65–73.
19 H. Zhang, K. H. Lu, M. Ebbini, P. Huang, H. Lu and L. Li, *npj Imaging*, 2024, **2**, 20.
20 B. G. Anderson, P. Popov, A. R. Cicali, A. Nwamba, C. R. Evans and R. T. Kennedy, *Anal. Chem.*, 2024, **96**, 16387–16396.
21 N. Plock and C. Kloft, *Eur. J. Pharm. Sci.*, 2005, **25**, 1–24.
22 M. G. Stovell, A. Helmy, E. P. Thelin, I. Jalloh, P. J. Hutchinson and K. L. H. Carpenter, *Front. Neurol.*, 2023, **14**, 1085540.
23 X. Wang, G. Rong, J. Yan, D. Pan, L. Wang, Y. Xu, M. Yang and Y. Cheng, *ACS Appl. Mater. Interfaces*, 2020, **12**, 45763–45771.
24 G. Crişan, N. S. Sanda Moldovean-Cioroian, D. G. Timaru, G. Andrieş, C. Căinap and V. Chiş, *Int. J. Mol. Sci.*, 2022, **23**, 5023.
25 R. Chakravarty, H. Hong and W. Cai, *Mol. Pharm.*, 2014, **11**, 3777–3797.
26 T. Iwai, Y. Takahashi, H. Miyahara and A. Okino, *Anal. Sci.*, 2013, **29**, 1141–1145.
27 M. Aida, T. Iwai, Y. Okamoto, S. Kohno, K. Kakegawa, H. Miyahara, Y. Seto and A. Okino, *Mass Spectrom.*, 2017, **6**, S0075.
28 M. Aida, T. Iwai, Y. Okamoto, H. Miyahara, Y. Seto and A. Okino, *J. Anal. At. Spectrom.*, 2018, **33**, 578–584.
29 T. Iwai, A. Albert, K. Okumura, H. Miyahara, A. Okino and C. Engelhard, *J. Anal. At. Spectrom.*, 2014, **29**, 464–470.
30 T. Iwai, K. Kakegawa, M. Aida, H. Nagashima, T. Nagoya, M. Kanemori-Kataoka, H. Miyahara, Y. Seto and A. Okino, *Anal. Chem.*, 2015, **87**, 5707–5715.
31 M. Cernakova, G. M. Hobusch, G. Amann, P. T. Funovics, R. Windhager and J. Panotopoulos, *Sci. Rep.*, 2021, **11**, 17832.
32 N. Kawakubo, J. Takemoto, Y. Koga, Y. Hino, A. Tamaki, K. Kohashi, H. Ono, Y. Oda, S. Ohga and T. Tajiri, *Pediatr. Int.*, 2022, **64**, e15228.
33 J. Y. Sung, D. G. Na, K. S. Kim, H. Yoo, H. Lee, J.-h. Kim and J. H. Baek, *Eur. Radiol.*, 2012, **22**, 1564–1572.
34 D. G. Na, J. H. Baek, S. L. Jung, J. H. Kim, J. Y. Sung, K. S. Kim, J. H. Lee, J. H. Shin, Y. J. Choi, E. J. Ha, H. K. Lim, S. J. Kim, S. Y. Hahn, K. H. Lee, I. Youn, Y. J. Kim, H. S. Ahn, J. H. Ryu, S. M. Baek, J. S. Sim and C. K. Jung, *Korean J. Radiol.*, 2017, **18**, 217–237.

35 R. Snoeckx and A. Bogaerts, *Chem. Soc. Rev.*, 2017, **46**, 5805–5863.
36 S.-Z. Li, J.-P. Lim, J. G. Kang and H. S. Uhm, *Phys. Plasmas*, 2006, **13**, 093503.
37 Y. Ikehara, H. Sakakita, N. Shimizu, S. Ikehara and H. Nakanishi, *J. Photopolym. Sci. Technol.*, 2013, **26**, 555–557.
38 S. Kos, T. Blagus, M. Cemazar, G. Filipic, G. Sersa and U. Cvelbar, *PLoS One*, 2017, **12**, e0174966.
39 A. Shimatani, H. Toyoda, K. Orita, Y. Hirakawa, K. Aoki, J. S. Oh, T. Shirafuji and H. Nakamura, *PLoS One*, 2021, **16**, e0255861.
40 J.-G. Shin, B. J. Shin, E. Y. Jung, C.-S. Park, J. Y. Kim and H.-S. Tae, *Polymers*, 2020, **12**, 1939.
41 J. S. de Maar, A. M. Sofias, T. Porta Siegel, R. J. Vreeken, C. Moonen, C. Bos and R. Deckers, *Theranostics*, 2020, **10**, 1884–1909.
42 S. Giordano, L. Morosi, P. Veglianese, S. A. Licandro, R. Frapolli, M. Zucchetti, G. Cappelletti, L. Falciola, V. Pifferi, S. Visentin, M. D'Incalci and E. Davoli, *Sci. Rep.*, 2016, **6**, 37027.
43 J. G. Swales, J. W. Tucker, M. J. Spreadborough, S. L. Iverson, M. R. Clench, P. J. Webborn and R. J. Goodwin, *Anal. Chem.*, 2015, **87**, 10146–10152.